GOST: A Geometric-Optical Model for Sloping Terrains

Weiliang Fan, Jing M. Chen, Weimin Ju, and Gaolong Zhu

***Abstract*—GOST is a geometric-optical (GO) model for sloping terrains developed in this study based on the four-scale GO model, which simulates the bidirectional reflectance distribution function (BRDF) of forest canopies on flat surfaces. The four-scale GO model considers four scales of canopy architecture: tree groups, tree crowns, branches, and shoots. In order to make this model suitable for sloping terrains, the mathematical description for the projection of tree crowns on the ground has been modified to consider the fact that trees grow vertically rather than perpendicularly to sloping grounds. The simulated canopy gap fraction and the area ratios of the four scene components (sunlit foliage, sunlit background, shaded foliage, and shaded background) by GOST compare well with those simulated by 3-D virtual canopy computer modeling techniques for a hypothetical forest. GOST simulations show that the differences in area ratios of the four scene components between flat and sloping terrains can reach up to 50%–60% in the principal plane and about 30% in the perpendicular plane. Two case studies are conducted to compare modeled canopy reflectance with observations. One comparison is made against Landsat-5 Thematic Mapper (TM) reflectance, demonstrating the ability of GOST to model canopy reflectance variations with slope and aspect of the terrain. Another comparison is made against MODIS surface reflectance, showing that GOST with topographic consideration outperforms that without topographic consideration. These comparisons confirm the ability of GOST to model canopy reflectance on sloping terrains over a large range of view angles.**

***Index Terms*—Canopy structure, geometric-optical (GO) modeling, radiative transfer, remote sensing, sloping terrains.**

NOMENCLATURE

A	Vertical projected area of a quadrat.
B	Vertical projected domain area.
D	Number of trees in domain B.
$G(\theta)$	Projection of unit leaf areas.
H	Effective height.
h	Tree height $H_a + H_b + H_c$.
H_a	Height of the lower part of the tree (trunk space).
H_b	Height of cylinders.
H_c	Height of cones.
L	Leaf area index (LAI).
L_o	Mean LAI accumulated over the view or sun path within one tree crown.
L_t	Clumping-adjusted projected tree crown area index.
m	Mean number of trees in a quadrat.
m_1	Mean number of cluster per quadrat.
m_2	Cluster mean size.
n	Number of quadrats in domain B.
$N_t(\lambda)$	Gap number density function between canopies.
P_G	Probability of sunlit ground area in the view directions.
$P_{\rm gap}(\theta)$	Gap probability within a tree at angle θ.
P_{ig}	Probability of sunlit ground area.
P_{vg}	Probability of viewing ground area.
P_{vg_r}	Probability of viewing ground area for random tree distribution.
P_{vg_c}	Probability of viewing ground area for clustered tree (Neyman distribution).
P_T	Probability of viewing sunlit foliage.
$P(x)$	Poisson distribution.
$P_N(i; m_1; m_2)$	Neyman type-A distribution.
r	Radius of the tree crowns.
R	Total reflectance.
R_G	Ground reflectance.
R_T	Tree reflectance.
R_{ZG}	Shaded ground surface reflectance.
R_{ZT}	Shaded tree surface reflectance.
S	The projected sloping quadrat area in the view direction.
$\bar{s}(\theta)$	Mean path length within a crown.
$t_a(\theta)$	Tree crown surface area at θ.
V	Volume of a tree.
W_s	Mean width of element shadows cast inside tree crowns.
W_t	Characteristic mean width of tree crowns projected to the ground.
α	Half apex angle.
γ_E	Needle-to-shoot area ratio.
Ω_E	Clumping index for shoots.
Ω_t	Clumping index for trees.
λ	Gap size.

Manuscript received February 4, 2013; revised October 25, 2013; accepted October 30, 2013. Date of publication November 22, 2013; date of current version March 5, 2014. This work was supported in part by the National Science Foundation of China under Grant 41271352/D0106, by the National Basic Research Program of China under Grant 2010CB950704, and by the Chinese Academy of Sciences for Strategic Priority Research Program under Grant XDA05050602.

W. Fan and W. Ju are with the Jiangsu Provincial Key Laboratory of Geographic Information Science and Technology and with the International Institute for Earth System Science, Nanjing University, Nanjing, 210046, China.

J. M. Chen is with the Jiangsu Provincial Key Laboratory of Geographic Information Science and Technology and with the International Institute for Earth System Science, Nanjing University, Nanjing, 210046, China. He is also with the Department of Geography and Program in Planning, University of Toronto, Toronto, ON M5S 3G3, Canada (e-mail: jing.chen@utoronto.ca).

G. Zhu is with the Department of Geography, Minjiang University, Fuzhou 350108, China.

Digital Object Identifier 10.1109/TGRS.2013.2289852

$\lambda_{\min}$	Minimum gap size for having an illuminated surface.
ϕ_g	Azimuth angle of the sloping background.
ϕ_v	View azimuth angle.
ϕs	Solar azimuth angle.
ϕ_{gv}	Relative azimuth angle between the viewer and the sloping background.
ϕ_{sv}	Relative azimuth angle between the sun and the viewer.
ϕ_{sg}	Relative azimuth angle between the sun and the sloping background.
θ_g	Slope of the sloping background or zenith angle of the sloping background.
θ'_s	Solar zenith angle to the horizontal background.
θ_s	Solar incidence angle to the sloping background.
θ'_v	View zenith angle to the horizontal background.
θ_v	View zenith angle to the sloping background.
ξ	Angle difference between the sun and the viewer.
S_{PT}	Percentage of sunlit points in viewed points.

I. Introduction

THE vegetation structure significantly affects its exchanges of matter and energy with the atmosphere, and therefore, vegetation structural parameters are important basic data for global change research. Geometric-optical (GO) models, as one kind of forest reflectance models, are suitable for developing algorithms for vegetation structural parameter retrieval because of their emphasis on vegetation structure and its interaction with radiative transfer processes in the canopy [1]–[4].

GO models have been well developed in the 1990s and early 2000s with the addition of radiative transfer schemes to address the complex multiple scattering issues in the canopy [5]–[7]. In recent years, the attention of many GO modelers have been turned to the applications of GO models for retrieving structural parameters such as LAI, clumping index, crown closure, and crown diameter [8]–[13]. Moreover, GO models are also used for canopy background reflectance retrieval [14]–[16], microwave modeling [17], and LiDAR analysis [18]–[20].

Many studies have shown that complex terrains strongly influence the canopy reflectance detected by sensors [21]–[23]. However, GO models are generally based on geometric relationships among solar zenith angle, view zenith angle, and relative azimuth angle between the sun and the viewer. They are only suitable for retrieving structural parameters of forests growing on flat terrains; however, forests are often found over complex terrains, which are particularly common in China.

A GO model consists of mathematical expressions of the canopy structure and within-canopy radiative transfer processes. Complex terrains influence both expressions [24], [25]. However, GO models usually only consider geometries of canopy structural components on a flat background [1], [2], [26]–[28]. Topographic corrections are generally used to reduce the topography effects on canopy bidirectional reflectance [22], [29], [30]. However, these types of corrections aim only at image angular normalization [31] and are not based on fundamental mechanisms of the canopy radiative transfer and its interaction with the sloping background. Some studies have gone beyond these simple correction methods. For example, Schaaf *et al.* [24] attempted to establish a GO model suitable for sloping terrains based on the Li–Strahler GO model. This model transformed ellipsoidal crowns into spherical shapes in 3-D space to simplify the projection of these crowns on a sloping surface. However, this approach is not suitable for crowns that are different from the spherical shape. Combal *et al.* [31] pointed out that the model of Schaaf *et al.* [24] uses an implicit assumption that trees are perpendicular to the sloping surface and classified this type of models as Perpendicular to the Ground Vegetation Model. In reality, most trees grow vertically whether on a sloping surface. For applicability on complex terrains, it is necessary to establish a GO model considering the sloping canopy structure and radiative transfer mechanisms in the sloping canopy.

A GO model can be evaluated using observations against various outcomes of the model, including 1) modeled reflectance [2], [27], [32]; 2) inverted canopy parameters [1], [10], [33], [34]; and 3) modeled canopy gap fractions [2], [27], [35]. These outcome-based evaluations may not be sufficient because intermediate errors in producing an outcome could cancel each other. With the development of computer technology, 3-D virtual canopy modeling [36]–[38] could be an effective way to evaluate not only the outcome but also the intermediate modeling results, such as the fractions of the sunlit and shaded foliage and background. This new evaluation tool has allowed us to evaluate GOST in its various development stages.

In this paper, we focus on the development of a GO model suitable for sloping terrains (GOST) based on the four-scale GO model [27] developed for flat terrains. GOST considers a sloping canopy structure with trees growing vertically rather than perpendicularly to sloping surfaces. We make a comparison between GOST and a 3-D virtual computer model to prove that GOST has the ability to simulate the canopy gap fraction and area ratios of the four scene components (sunlit foliage, sunlit background, shaded foliage, and shaded background). The reflectance retrieved from a Landsat Thematic Mapper (TM) image and MODIS images are used to evaluate GOST performance.

II. Model Description

The reflected signals received by sensors are assumed to be composed of signals from four scene components: sunlit foliage (P_T), sunlit ground (P_G), shaded foliage (Z_T), and shaded ground (Z_G). The total canopy reflectance is

$$R = R_T \cdot P_T + R_G \cdot P_G + R_{ZT} \cdot Z_T + R_{ZG} \cdot Z_G \qquad (1)$$

where P_T and P_G are the sunlit components that intercept the direct sunlight, and Z_T and Z_G are the shaded components receiving only the diffuse radiation from the sky and scattered radiation in the canopy. R_T, R_G, R_{ZT}, and R_{ZG} are the reflectance factors of the four scene components in GOST.

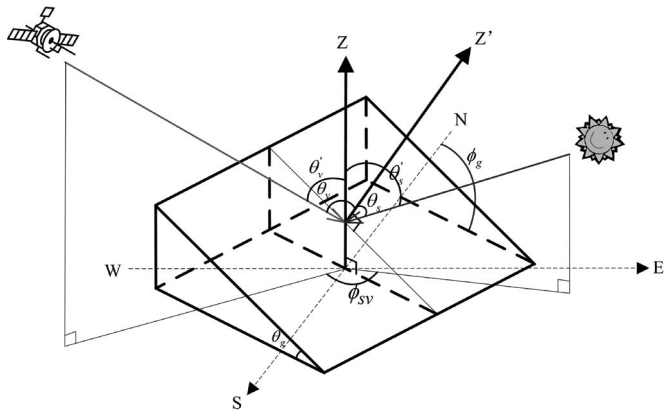

Fig. 1. Coordinate system of photon interaction with a canopy on a sloping background. E, S, W, and N are the east, south, west, and north directions to the horizontal ground. Z is the vertical direction to the horizontal ground. Z' is the vertical direction to the sloping ground.

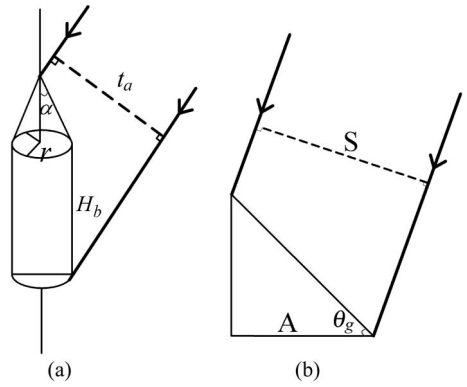

Fig. 2. Projections of tree crown and background. (a) Projection area t_a of a tree crown in the sunlight or viewer direction. (b) Projection area S of the sloping background in the sunlight or viewer direction. The arrow directions are the sunlight or viewer directions.

Here, the vegetation and background components in the view direction will be first separated based on the gap fraction, and the four scene components will then be separated on sloping terrains.

A. Determining the Coordinate System for a Sloping Canopy

GO models, such as the four-scale GO model, assume that trees are perpendicular to the background surface. The projection of tree crowns on the background is described using the solar zenith angle (θ_s'), view zenith angle (θ_v'), and relative azimuth angle between the sun and the viewer (ϕ_{sv}) for the horizontal surface. In GOST, the projection of forest scene components on sloping terrains is described using additional angles, including the solar incidence angle to the sloping surface $(\theta_s, \cos(\theta_s) = \cos(\theta_g)\cos(\theta_s') + \sin(\theta_g)\sin(\theta_s')\cos(\phi_{sg}))$, view incidence angle to the sloping surface $(\theta_v, \cos(\theta_v) = \cos(\theta_g)\cos(\theta_v') + \sin(\theta_g)\sin(\theta_v')\cos(\phi_{gv}))$, and slope (θ_g) and aspect (ϕ_g) (see Fig. 1).

B. Tree Distribution

The canopy gap size and gap fraction distributions are determined by the tree distribution. Chen and Leblanc [27] studied both the random Poisson distribution and the nonrandom Neyman type-A distribution [39] for describing the tree distribution. The results showed that the Neyman type-A distribution is better than the Poisson distribution in capturing a tree distribution pattern in a boreal forest. However, the Poisson distribution can be used as a backup approach when detailed tree distribution data are lacking. These two distributions are alternatively used in GOST, and other types of distributions can also be used to replace them. In GOST, a study area is divided into a number of quadrats in order to obtain a statistical tree distribution. The Poisson distribution is

$$P(x) = \frac{e^{-m}m^x}{x!} \tag{2}$$

where $P(x)$ is the probability of finding x trees in a quadrat. m is the mean number of trees in a quadrat. In order to avoid overly populated quadrats that could be difficult to handle numerically, Chen and Leblanc [27] gave an example: For a 100 × 100 m domain with 3000 trees, it is preferable to divide the domain into at least ten quadrats.

The Neyman type-A distribution assumes that trees are first combined in clusters, and the spatial distribution of the center of a cluster follows the Poisson process, that is

$$P_N(i; m_1; m_2) = e^{-m_1}\frac{m_2^i}{i!}\sum_{j=1}^{\infty}\frac{[m_1 e^{-m_2}]^j}{j!}\cdot j^i \qquad i = 0, 1, 2, \cdots \tag{3}$$

where $P_N(i; m_1; m_2)$ is the probability of finding i trees in a quadrat, m_1 is the mean number of clusters per quadrat, m_2 is the cluster mean size, and j is the cluster number in a quadrat.

The tree crown distribution on sloping terrains is assumed to be the same as that on a flat terrain at nadir, and the number of tree crowns projected in the vertical direction is assumed to be invariant on different slopes.

C. Projection of Tree Crowns on the Sloping Background

In GO models, a tree is generally assumed to be an ideal 3-D geometric shape according to the geometric characteristics of tree species, such as cone [1], [32], ellipsoidal [28], [40], and "cone + cylinder" [27]. Rautiainen *et al.* [41] indicated that the shape of tree crowns is one of the key parameters for determining the canopy bidirectional reflectance. The "cone + cylinder" shape is used in GOST for coniferous tree crowns. However, other geometric shapes can also be used to replace it as needed.

The projection of tree crowns on the background is the basis to model the scene components using a GO approach. For the purpose of designing the new projection relationship, the "cone + cylinder" projected area t_a [see Fig. 2(a)] and sloping background projected area S [see Fig. 2(b)] in the viewer and sunlight directions should be considered. Therefore, tree crowns are projected onto the sloping background in GOST using t_a/S in the sunlight and view directions, separately.

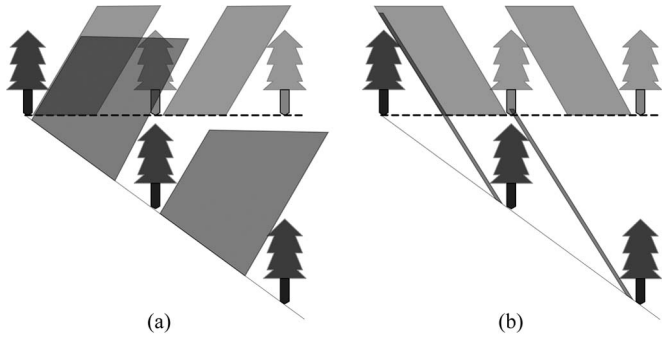

Fig. 3. Topographic effects on the gap size. (a) If the sunlight or view direction is facing the sloping background, the gap fraction and gap size between crowns increase with the increasing slope. (b) If the sunlight or viewer direction is not facing the sloping background, the gap fraction and the gap size between crowns decrease with the increasing slope.

The "cone + cylinder" projected area in the view direction is

$$t_a\left(\theta_v'\right) = \begin{cases} \pi r^2 + 2r\sin\left(\theta_v'\right) H_b & \theta_v' = 0 \\ \pi r^2 \cos\left(\theta_v'\right) + 2r\sin\left(\theta_v'\right) H_b & \theta_v' < \alpha \\ \pi r^2 \cos\left(\theta_v'\right) + t_{act} + 2r\sin\left(\theta_v'\right) H_b & \theta_v' > \alpha \end{cases} \tag{4}$$

where r is the radius of the tree crowns, H_b is the height of cylinders, α is the half apex angle, and t_{act} is the top part of the tree crown projected area in the view direction (see the Appendix). Using θ_s' instead of θ_v', (4) gives the "cone + cylinder" projected area in the sunlight direction.

The projected sloping quadrat area in the view direction is

$$S = A \cdot \cos(\theta_v) / \cos(\theta_g) \tag{5}$$

where A is the projected quadrat area at nadir, and $A/\cos(\theta_g)$ is the sloping background area. Using θ_s instead of θ_v, (5) gives the projected sloping area in the sunlight direction.

D. Separating Foliage and Background on Sloping Terrains

The gap fraction is used to separate foliage and background on sloping terrains in GOST. In forest canopies, leaves are clumped within tree crowns, and trees are grouped rather than randomly distributed. Therefore, the gap fraction within a canopy is composed of those between and within tree crowns.

Fig. 3 shows that the gap fraction of a canopy is strongly influenced by sloping terrains. The new projection t_a/S is used for calculating the gap fraction between crowns on sloping terrains. In the view direction, the gap fraction between crowns in a sloping quadrat is described using the Poisson distribution, i.e.,

$$P_{vg\_r} = \left[1 - \frac{t_a\left(\theta_v'\right)}{S}\right]^{D/n} \tag{6}$$

and the gap fraction between crowns calculated using the Neyman type-A distribution $P_N(i; m_1; m_2)$ on sloping terrains is

$$P_{vg\_c} = \sum_{i=0}^{k} P_N(i; m_1; m_2) \left[1 - \frac{t_a\left(\theta_v'\right)}{S}\right]^i \tag{7}$$

where D is the number of trees in domain B, n is the number of quadrats in domain B, and k is an integer that should be large enough to consider all overlapped trees in a quadrat and is equal to 350 here. Using θ_s' instead of θ_v', (6) and (7) give the gap fractions between crowns corresponding to the Poisson (P_{ig_r}) and Neyman type-A (P_{ig_c}) distributions in the sunlight direction, separately.

Lambert–Beer's law is generally used for describing the transmission of beam radiation [42]–[44]. Chen and Leblanc [27] used an equation similar to that used by Li and Strahler [35] but modified it to consider the foliage clumping effect [45] for simulating the gap fraction within a tree. In GOST, the function used in the four-scale model to calculate gap fraction for a tree is modified. Different from the gap fractions between tree crowns, the gap fraction within a tree does not change with the slope of the background. Therefore, the gap fraction in a tree in the view direction is

$$P_{\text{gap}}\left(\theta_v'\right) = e^{-G(\theta_v')L_0\Omega_{\text{E}}/\gamma_{\text{E}}} \tag{8}$$

where $G(\theta_v')$ is the projection of unit leaf area, which is equal to 0.5 for a spherical leaf angle distribution [27], [46]. Ω_E is the clumping index for shoots, quantifying clumping at scales larger than the shoot. γ_E is the ratio of half total needle area in a shoot to half total shoot surface area [46]. L_0 is the LAI in the view direction and calculated as $L_0 = \mu \cdot \overline{s}$, where μ is the foliage volume density ($\mu = L/[V \cdot D/B]$). For sloping terrains considered here, L is defined as one half the total leaf area per unit horizontally projected ground surface area (LAI). Therefore, according to the assumption that the tree crown is vertically grown, LAI does not change with the slope of background at nadir. B is the vertically projected domain area at nadir, and V is the volume of a tree crown. $\overline{s}$ is the mean of path length through a tree. In the view direction, it is calculated as $\overline{s}(\theta_v') = V/t_a(\theta_v')$.

The total gap fraction over a sloping terrain is

$$P_{vg} = \sum_{j=1}^{k} P_{tj}(t_a) P_{\text{gap}}^{j}\left(\theta_v'\right) + P_{vg\_c} \tag{9}$$

where $P_{\text{gap}}^{j}(\theta_v')$ is the gap probability within a canopy with j trees overlapping along the view line and calculated as

$$P_{\text{gap}}^{j}\left(\theta_v'\right) = \prod_{1}^{j} P_{\text{gap}}\left(\theta_v'\right). \tag{10}$$

In (9), $P_{tj}(t_a)$ is the probability of j trees intercepting the view line and calculated using the binomial distribution, i.e.,

$$P_{tj}(t_a) = \sum_{i=j}^{k} P_N(i; m_1; m_2) \frac{i!}{(i-j)!j!} \times \left[1 - \frac{t_a\left(\theta_v'\right)}{S}\right]^{i-j} \left[\frac{t_a\left(\theta_v'\right)}{S}\right]^{j}. \tag{11}$$

With θ_s' instead of θ_v', (9) can also be used to calculate the gap fraction in the sloping canopy in the sunlight direction P_{ig}.

E. Separating Sunlit and Shaded Backgrounds on Sloping Terrains

P_{ig} represents the sunlit background fraction, and P_{vg} is the viewed background fraction. If the view line and solar beam penetrations through the canopy are independent of each other, the fraction of sunlit background in the view direction is simply the product of P_{ig} and P_{vg}. However, when the view line is near the solar beam direction, it can penetrate through the same gap in the canopy as the solar beam and increases the probability of observing the sunlit background. A hotspot occurs when the view line is in the same direction as the solar beam. Chen and Leblanc [27] proposed a hotspot function on a horizontal surface. In GOST, the form of the hotspot function is the same as that of the four-scale model. However, some variables are modified here to be suitable for sloping terrains. The hotspot function is

$$F_t(\xi) = \frac{\int_{\lambda_{\min}}^{\infty} \left[1 - \frac{\xi}{\tan^{-1}(\lambda/H)}\right] N_t(\lambda) d\lambda}{\int_{\lambda_{\min}}^{\infty} N_t(\lambda) d\lambda} \tag{12}$$

where the angle between the sun and the viewer (phase angle) is

$$\xi = \arccos\left(\cos\left(\theta_v'\right)\cos\left(\theta_s'\right) + \sin\left(\theta_v'\right)\sin\left(\theta_s'\right)\cos(\phi_{sv})\right). \tag{13}$$

H is the effective height given as $(H_a + H_b + H_c/3) \times \cos(\theta_g)/\cos(\theta_s)$, H_a is the height of the lower part of the tree (trunk space), H_b is the height of cylinders, and H_c is the height of cones.

$N_t(\lambda)$ is the gap number density given as

$$N_t(\lambda) = \frac{L_t}{W_t} e^{-L_t[1+(\lambda/W_t)]}. \tag{14}$$

The characteristic mean width of a tree projected in the sunlight direction is

$$W_t = \sqrt{t_a\left(\theta_s'\right)}. \tag{15}$$

The clumping-adjusted projected crown area index on sloping terrains is

$$L_t = \Omega_t t_a\left(\theta_s'\right) D/\left(B\cos(\theta_s)/\cos(\theta_g)\right). \tag{16}$$

Ω_t is a tree clumping index, determined by the Neyman distribution defined as

$$\Omega_t = \log\left(P_{ig\_c}(\text{Neyman})\right)/\log\left(P_{ig\_r}(\text{Poisson})\right). \tag{17}$$

For a given angle difference between the sun and the viewer, there is a minimum gap size $\lambda_{\min}$ in which the view line penetrates through the same gap as the solar beam, determined by

$$\lambda_{\min} = H\tan(\xi). \tag{18}$$

λ is the gap size of the canopy between $\lambda_{\min}$ and ∞.

Therefore, the total probability of seeing the sunlit background on sloping terrains is

$$P_G = P_{ig}P_{vg} + [P_{ig} - P_{ig}P_{vg}]F_t(\xi). \tag{19}$$

The first term on the right-hand side represents the probability of observing the sunlit background when the view line penetration is independent of the solar beam penetration, and the second term is the enhanced probability due to the hotspot.

The probability of seeing the shaded background on sloping terrains is

$$Z_G = P_{vg} - P_G. \tag{20}$$

It is the difference in the probabilities of observing the total background (P_{vg}) and the sunlit background (P_G).

F. Separating Sunlit and Shaded Foliage on Sloping Terrains

The separation of sunlit and shaded foliage in the view direction presents a challenge in forest GO modeling. There is still no perfect geometric description for this purpose. In GOST, a simplified ray tracing method is developed for separating sunlit and shaded foliage on sloping terrains. The basic idea of this method is first to describe the foliage spatial and angular distributions and then to penetrate a view line into the canopy. If the view line can touch any foliage in the canopy, we need to determine whether the sunlight can reach the same point of the foliage. Through repeating these aforementioned steps many times, the probability of viewing sunlit foliage can be separated from the viewed foliage.

A variety of foliage shapes and crown shapes can be used for separating sunlit and shaded foliage using straightforward geometric formulas of the simplified ray tracing method depending on forest types. Specific distributions of foliage and crowns can also be used here according to the measured data in forests. However, large amounts of needle foliage of conifer trees need large computer memory space, which greatly exceeds the capacity of a personal computer. For this reason, a shoot is treated as the minimum foliage element. The shape of foliage can be treated not only to be planar shapes, such as circular, square, rectangle, rhombus, and so on, but also 3-D shapes, such as cylinder, cuboid, hexagonal prism, and so on. In order to reduce the number of facets of a forest scene, the planar shape of foliage is used for both the broad leaved and conifer forest scenes in the simplified ray tracing method. In general, the planar shape of foliage is suitable for broadleaf forests. For conifer forests, the projection coefficient of flat leaves in a given direction is the same as that of spheres (representing shoots) as long as they are all randomly distributed in space, and the definition of half the total area is used [45]. This means that the results of ray tracing based on the planner shape are directly applicable to the shoots when half of the total plane area (both sides) is used to represent half the total shoot area (average projected shoot area $\times\,\pi$). The needle-to-shoot area ratio is then used to convert this half the total needle area to half the total shoot area. In this way, the ray tracing results for the planner leaf shape can be used for both broadleaf and needleleaf forests.

An example is used to explain how to use the simplified ray tracing method for separating sunlit and shaded foliage. This method needs to determine the forest scene on slopes first. In describing the foliage spatial and angular distributions, we assume crowns to be randomly distributed in space and leaves

to be randomly distributed within each crown. The crown is assumed to be "cone + cylinder," and the foliage is assumed to be circular and flat plates. A vector normal to the plate is used for describing the foliage angular distribution [47]. The foliage spatial distribution in a tree is expressed using the random centers of these plates. According to the center and normal vector of a plate, the direction and position of it can be determined. In the ray tracing procedure, the view azimuth angle ϕ_v is set to zero. The sunlight direction, slope and aspect of the terrain, and the view zenith angle $\theta'_{\rm v}$ are varied to simulate multiangular views. In these simulations, a plane, which is perpendicular to the direction vector of the view line, can be determined by any specific point far from the top of the forest canopy. In order to make all the view lines penetrating into the forest scene, only a rectangle region in the plane is used as the launch positions of the view lines according to the range of the forest scene. The number of the incident view lines can be determined by the foliage density in a specific forest scene. In general, the denser the foliage in a forest scene, the more incident view lines are required. For this reason, the number of the incident view lines can be related to LAI. In general, we recommend that the number of the incident view lines is no less than 10 000 for each forest scene, which contains no more than 100 crowns with LAI of about 3. Second, the view lines are sent from the launch positions of the plane to the forest scene one by one. If a view line does not touch any plates in the forest scene, it is not considered. Otherwise, the first intersection point (FIP) of the view line and the plate could be found. To eliminate the edge effect, only the incident view lines that reach a relatively small square center area of the forest scene are preserved. Third, if the sight line intersects with a plate, we need to decide whether the FIP can be touched by the sunlight according to the direction vector of the sunlight and the normal vector of the plate. If there exists another plate between the sun's position and the FIP or the FIP is not in the same side of the plate hit by the sunlight, the FIP is a shaded point in the view direction. Otherwise, it is a sunlit point in the view direction.

After all the ray tracing procedure, we can get the percentage of sunlit points that are reached by the view lines S_{PT} in the view direction. The total probability of seeing the sunlit foliage in the sloping canopy is

$$P_T = S_{PT}/(1 - P_{vg}). \tag{21}$$

The total probability of seeing the shaded foliage in the sloping canopy is

$$Z_T = 1 - P_{vg} - P_T. \tag{22}$$

III. Results and Analysis

The area ratios of the four scene components of a sloping forest are conceptual quantities, which are difficult to observe in real forest canopies. Therefore, the 3-D virtual canopies are constructed using a computer graphics technique to evaluate the simulated area ratios by GOST. Then, the reflectance simulated by GOST is compared with the reflectance data retrieved from a TM image and from a MODIS multiangle surface reflectance product over a mountainous area in China for the purpose of evaluating the performance of GOST.

TABLE I
Canopy Parameters for Simulating the Area Ratios of the Four Scene Components by the 3-D Virtual Model and GOST

LAI	Ha	Hb	r	α	Ws	Ω_E	γ_E	G(θ)
2.7	0.5 m	2.5 m	0.85 m	30°	0.17 m	1	1	0.5

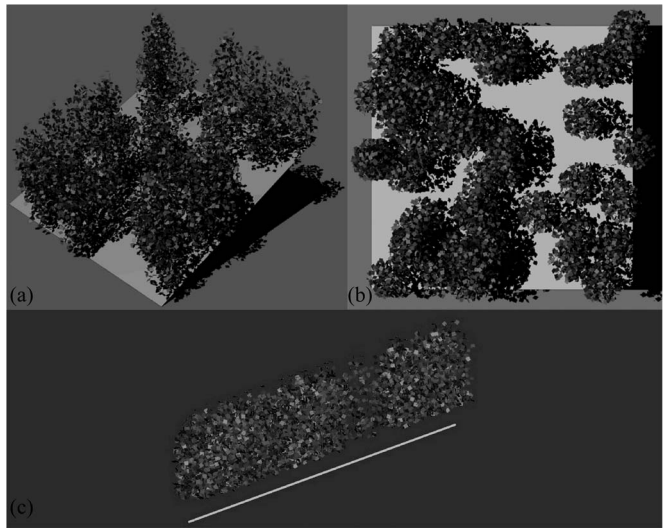

Fig. 4. Example of a 3-D virtual canopy on a 20° slope. This 3-D virtual canopy is produced using the 3-D max software and the Maxscript computer language. The rendered scenes are classified as the four scene components in multiangle directions. (a) Perspective view. (b) Nadir view. (c) Side view.

A. Model Comparison

In GOST, the sunlit and shaded foliage fractions that are seen in a given direction are separated based on the geometrical shape of the tree crown and the probability of solar beam and view line penetrations within the crown. The separation of the four scene components is a fundamental part of GO modeling and is checked against ray tracing in 3-D virtual canopies. As the principles of GO modeling for broadleaf and conifer canopies are similar, we choose broadleaf virtual canopies for this purpose, which are structurally less complex and require less computation than conifer canopies.

1) Virtual Canopy Modeling: The 3-D max software and the Maxscript computer language are used for constructing 3-D virtual canopy models to compare the area ratios of the four scene components on sloping terrains calculated using GOST. A 3-D virtual canopy consists of broad leaves that are randomly distributed within a crown. The virtual tree crowns are distributed on a sloping quadrat randomly in the vertical direction. A virtual forest scene is then separated into sunlit and shaded parts under the virtual parallel sunlight in the 3-D max camera view. The multiangle images of the virtual canopy are rendered using axonometric projection through moving the positions and changing the view angles of the 3-D Max camera. Finally, the four scene components are classified in each of the rendered multiangle images of a virtual canopy. The regions that are not influenced by edge effects are artificially selected to classify the four scene components in these rendered multiangle images.

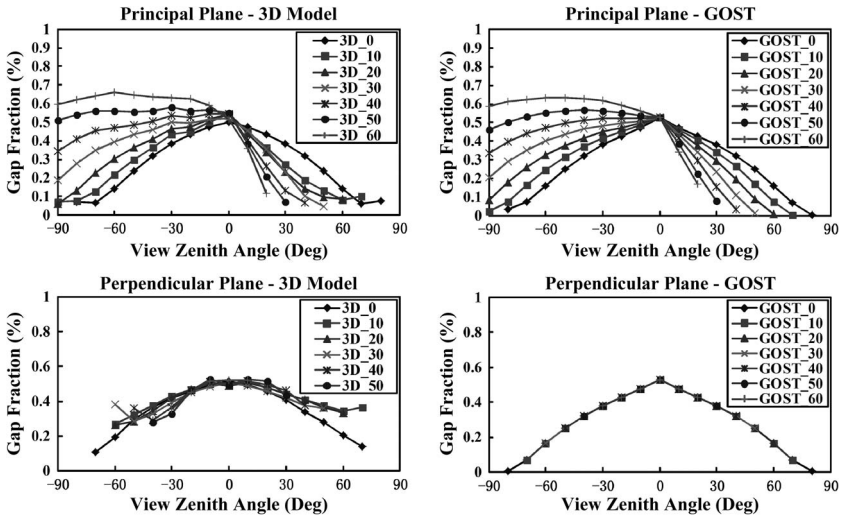

Fig. 5. Comparison of the classified and simulated gap fractions of the sloping canopies ($\phi_g = 0$) in the principal and perpendicular planes. 3D_0, 3D_10, 3D_20, 3D_30, 3D_40, 3D_50, and 3D_60 are the simulated results of the 3-D virtual canopy model with the slope of the background at 0°, 10°, 20°, 30°, 40°, 50°, and 60°. GOST_0, GOST_10, GOST_20, GOST_30, GOST_40, GOST_50, and GOST_60 are the simulated results of GOST with the slope of the background at 0°, 10°, 20°, 30°, 40°, 50°, and 60°.

2) Forest Site Example: A set of broadleaf canopy parameters in reasonable ranges is shown in Table I as the inputs to the 3-D virtual canopy model and GOST. Because it is time consuming to simulate the detailed forest scenes, only 1/4 of a quadrat (125 m^2) with 50 tree crowns is simulated. In this example, a virtual leaf is assumed to be a circular and flat plate with diameter W_s. The solar zenith angle θ_s' and solar azimuth angle ϕs are set to 30° and 180°, respectively. The azimuth angle ϕ_g of the sloping background is set to zero. An example of the 3-D virtual canopy on a 20° slope is shown in Fig. 4.

Fig. 5 shows how the gap fraction changes with background slope from 0° to 60° in 10° intervals in the principal and perpendicular planes. The relative azimuth angle between the sun and the viewer equals 0° or 180° in the principal plane and 90° in the perpendicular plane. The comparison shows that the gap fractions simulated by GOST agree well with the outputs from the 3-D virtual canopy model. It indicates the ability of GOST to separate the foliage components and the background components on sloping terrains.

Different from trees growing on flat terrains, sloping canopies cannot be observed from all view angles of the hemisphere (see Fig. 3). For example, the range of the view zenith angle decreases with increasing slope of the inclined background in the principal plane (see Fig. 5). In the perpendicular plane, the absence of the gap fraction simulated by the 3-D virtual canopy model is because the tree-covered regions are too small to be classified in the rendered images at large θ_v.

Both GOST and the 3-D virtual canopy model assume that the number of tree crowns does not change with the slope of terrains in the vertical direction. Therefore, the simulated gap fraction also does not change with the slope at nadir (see Fig. 5). In the principal plane, the gap fraction increases on the backscattering side (negative θ_v') and decreases on the forwardscattering side (positive θ_v') with the slope of the inclined background because θ_v values are different on both sides of the vertical direction. The gap fractions are also not the same on different slopes in the same view direction. On the backscattering side, the gap fraction increases with slope in the same view direction. On the contrary, on the forwardscattering side, the gap fraction decreases with increasing slope in the same view direction. Gap fractions on both sides of the perpendicular plane are the same because the forest scene components are symmetric on both sides of the vertical direction when the relative azimuth angle equals 90°. The gap fraction reaches a maximum at nadir in the perpendicular plane because the overlapping of tree crowns is minimum in this view direction. With the increase in the view zenith angle, the overlapping of tree crowns increases, and the gap fraction decreases with slope. Moreover, the gap fraction does not change with slope of the inclined background at the same θ_v' on both sides of the perpendicular plane because $\cos(\phi_{gv}) = 0$ and the projected area of background S and the projected area of a tree crown $t_a(\theta_v')$ do not change with slope.

Different from the outputs of GOST, the classified gap fractions by the 3-D virtual canopy model are unsmooth (see Fig. 5). Such as the sudden rise in gap fractions at 0° and 10° slopes in the principal plane and the unsmooth gap fractions at large slopes in the perpendicular plane. There are also unsymmetric gap fractions that are simulated by the 3-D virtual forest on both sides of the vertical direction in the perpendicular plane. These unsmooth and unsymmetric results are caused by the insufficient number of trees included in the simulation where a few tree crowns can have unproportionally large contributions to the view in certain directions. However, the simulated gap fractions by GOST are smooth and symmetric both in the principal and perpendicular planes. This model comparison demonstrated that the results of the 3-D virtual canopy model and GOST have no systematic deviation, and GOST has the ability to separate foliage and background area ratios (gap fraction) of forest on slopes.

The area ratios of the four scene components modeled by GOST are very close to those simulated by the 3-D virtual canopy model in both principal and perpendicular planes (see Figs. 6 and 7). It indicates that both models have no systematic

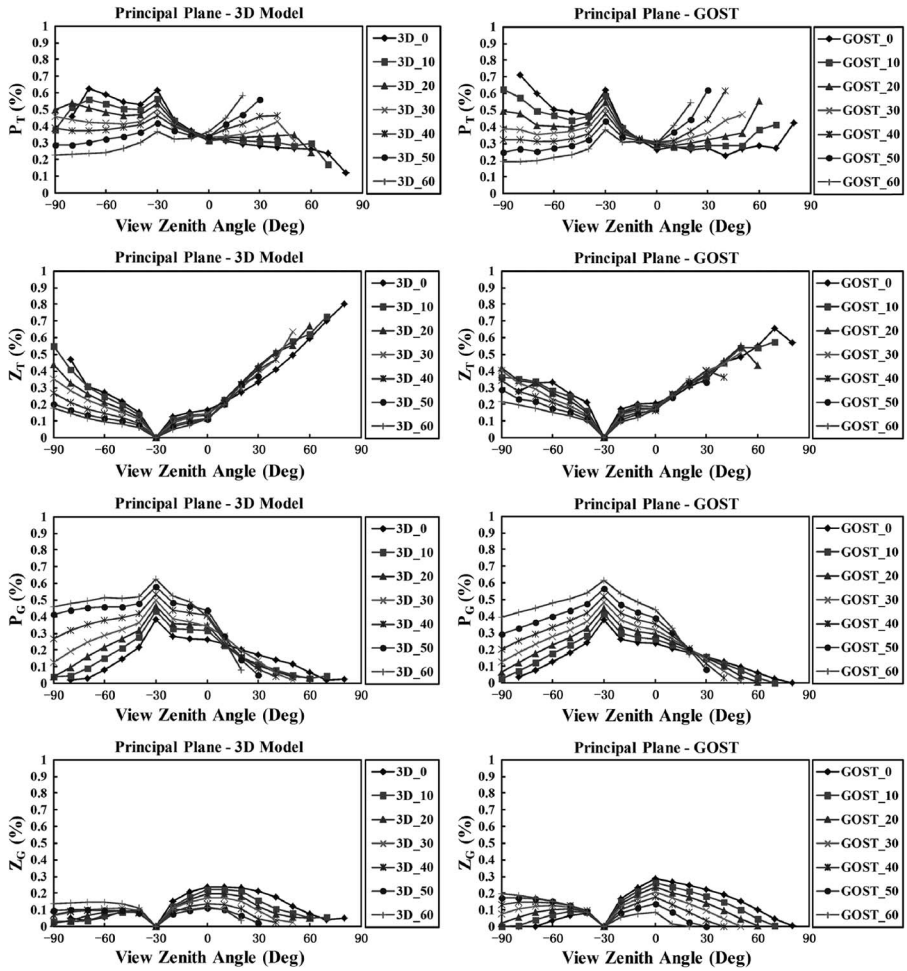

Fig. 6. Comparison of the classified and simulated four scene components area ratios of the sloping canopy in the principal plane. 3D_0, 3D_10, 3D_20, 3D_30, 3D_40, 3D_50, and 3D_60 are the simulated results of the 3-D virtual canopy model with the slope of the background at 0°, 10°, 20°, 30°, 40°, 50°, and 60°. GOST_0, GOST_10, GOST_20, GOST_30, GOST_40, GOST_50, and GOST_60 are the simulated results of GOST with the slope of the background at 0°, 10°, 20°, 30°, 40°, 50°, and 60°.

deviation, and GOST has the ability to separate the four scene components area ratios of sloping canopies. In addition, a total of 8500 view lines are emitted from the launching plane to the forest scene by GOST for separating sunlit and shaded foliage on each slope and in each view direction. The average computing time for separating the four scene components is only 8 s, and therefore, GOST is a useful method despite the fact that it contains a simplified ray tracing process. GOST can explicitly represent the topographic effects on area ratios of foliage components because it considers the sloping canopy structure in any view directions. These simulations show that the differences in the area ratios of the four scene components between flat and sloping terrains can reach up to 50%–60% in the principal plane and about 30% in the perpendicular plane (see Figs. 6 and 7). Therefore, without considering the effects of sloping terrains in GO models, it might cause significant errors in the area ratios of the four scene components, and the errors are consequently passed to the simulated canopy reflectance.

When the view and sunlight directions are the same, the "hotspot" occurs in the principal plane (see Fig. 6). The hotspot is an important phenomenon that can be used for retrieving canopy structural parameters, such as clumping index [8], [48]. GOST successfully simulates significant increases in the area ratios of sunlit foliage and background components at the hotspot. The shaded foliage and background area ratios are 0% at the hotspot because these two scene components cannot be observed at the hotspot. In the hotspot direction, the gap fraction increases with slope, and therefore, the sunlit and shaded foliage area ratios decrease.

The variation of the sunlit foliage area ratio reaches the minimum at different slopes at nadir at which the overlapping of tree crowns reaches the minimum. The gap fraction increases with slope in the backscattering side of the principal plane. Therefore, foliage area ratios decrease with increasing slope. On the contrary, the gap fraction decreases, and foliage area ratios increase with slope in the forwardscattering side. Fig. 6 also shows that both the classified and simulated foliage area ratios are unsmooth in the principal plane, particularly at large view zenith angles θ_v. The reason of the unsmooth results classified by the 3-D virtual canopy model is the small portion of the image that can be rendered at large view zenith angles at which it is difficult to class the foliage area ratios. However, the unsmooth foliage area ratios simulated by GOST are caused by the small forest scene that contains an insufficient number of trees to be statistically representative at all angles. The gap fraction increases with slope in the backscattering direction,

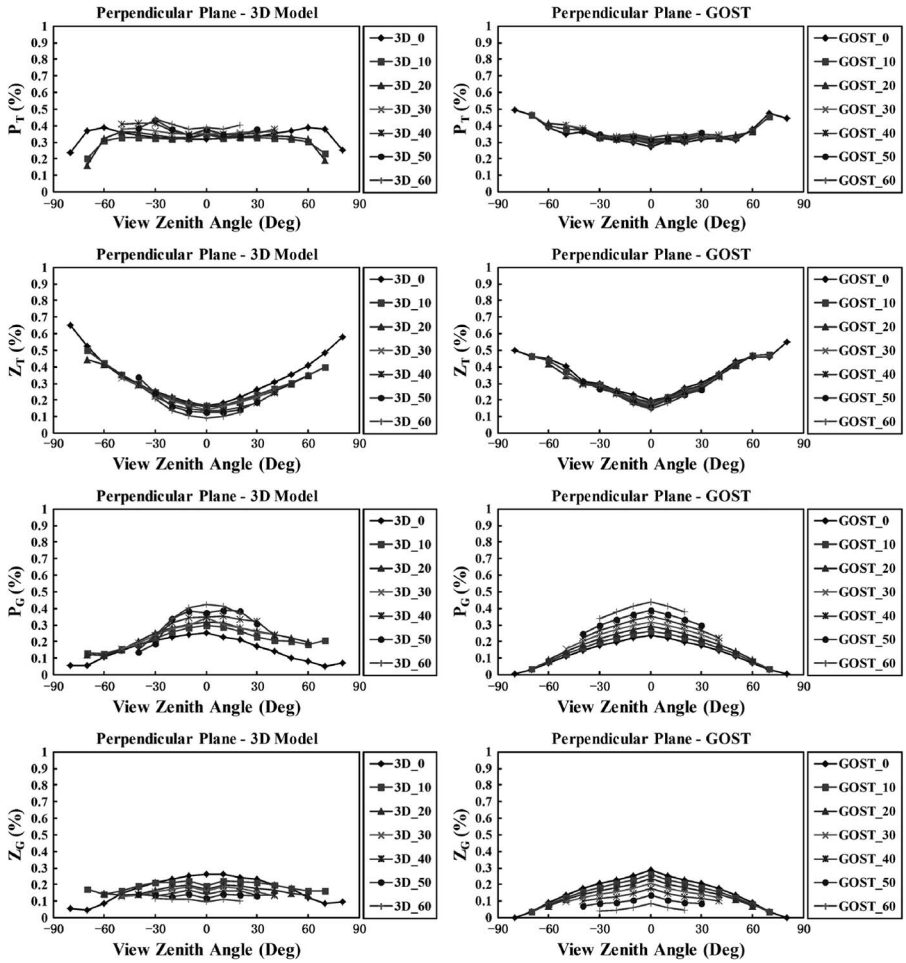

Fig. 7. Comparison of the classified and simulated four scene components area ratios of the sloping canopy in the perpendicular plane. 3D_0, 3D_10, 3D_20, 3D_30, 3D_40, 3D_50, and 3D_60 are the simulated results of the 3-D virtual canopy model with the slope of the background at 0°, 10°, 20°, 30°, 40°, 50°, and 60°. GOST_0, GOST_10, GOST_20, GOST_30, GOST_40, GOST_50, and GOST_60 are the simulated results of GOST with the slope of the background at 0°, 10°, 20°, 30°, 40°, 50°, and 60°.

and therefore, the sunlit background area ratio increases with slope. The gap fraction does not change with slope in the nadir view direction; as a consequence, the sunlit background area ratio increases, and the shaded background area ratio decreases with increasing slope. The sunlit background area ratio has the least influence at about 20° view zenith angle (θ'_v). This is because the sunlit background area ratio increases with slope and decreases with increasing view zenith angle, and the balance is achieved at this θ'_v. In the 3-D virtual canopy, the uncertainty of the shaded background area ratio comes from the accumulative error because the shaded background area ratio is equal to the gap fraction minus the sunlit background area ratio.

Fig. 7 also shows the unsmooth foliage area ratios classified by the 3-D virtual canopy model in the perpendicular plane, particularly the sudden decrease in the sunlit foliage area ratio at large θ_v. The sunlit background area ratio increases with slope in the perpendicular plane because more sunlight reaches the background through a canopy. Therefore, the shaded background area ratio decreases with increasing slope. In the perpendicular plane, the gap fraction decreases with increasing θ'_v, and therefore, sunlit and shaded foliage area ratios increase with θ'_v. Despite the unsymmetric and unsmooth sunlit and shaded background area ratios on both sides of the vertical direction in the perpendicular plane, the classified background area ratios by the 3-D virtual canopy model are close to the simulated results by GOST. It indicates that GOST can separate sunlit and shaded backgrounds on slopes with reasonable accuracy.

B. Model Validations

In order to prove the ability of GOST to model canopy reflectance variations with slope and aspect of the terrain, two experiments are designed for validating the reflectance simulated by GOST. Considering the difficulty in observing the canopy parameters on slopes, we use best estimates of common canopy parameters to fit the observed reflectance acquired from remote sensing images.

1) Comparison of the Modeled and Landsat Reflectance: In this experiment, the reflectances of many pixels in a Landsat TM5 image are needed to enhance the regularity of the reflectance variation with slope. Therefore, a rectangle forest region (94 581 m × 123 375 m) northeast of China (near 53N, 124E) is selected as the study site. The vegetation cover is predominantly conifer forest in this region. The corresponding Landsat TM5 image is acquired on August 30, 2009, and

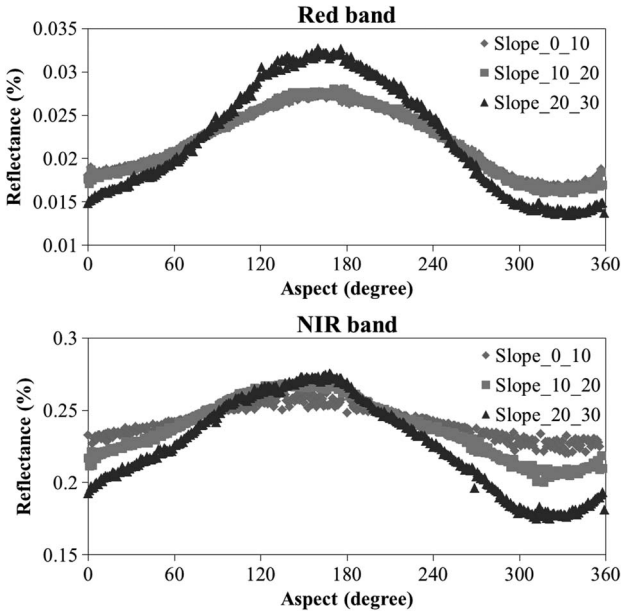

Fig. 8. Observed reflectance in the TM5 image (the red and NIR reflectance) varies with slope and aspect of the terrain. The blue, green, and red dots represent the slope between 0° and 10°, between 10° and 20°, and between 20° and 30°, respectively.

a total of 3153 × 4113 nadir view pixels are selected for this study. However, no ground observations are available for the sloping canopy parameters corresponding to these selected pixels. Therefore, the direct comparisons of the statistical results from the Landsat TM5 image and the model simulated results cannot be made. In this experiment, the quantitative analysis of the topographical effects on the sloping canopy reflectance is based on model simulated results, and the observed Landsat TM reflectance data are used to support the model simulated results.

Spectral reflectance in the red and NIR bands is retrieved from the original digital number of the Landsat TM5 image. The solar azimuth angle is 154°, and the solar zenith angle is 46° of this TM5 image. The digital elevation model (DEM) data sets for this study site are used to produce images of the slope and aspect. The slope is divided into three intervals: from 0° to 10°, from 10° to 20°, and from 20° to 30°. The aspect ranges from 0° to 359° in 1° intervals. Then, the mean values of reflectance are computed for each slope and aspect interval. The statistical results of the TM5 image are shown in Fig. 8.

We have made a best estimate of the model inputs using common parameter values of forest within reasonable ranges. In this case, conifer trees are simulated as "cone + cylinder" with the Neyman distribution. The slopes of 5°, 15°, and 25° are used for simulating the reflectance to represent the slope between 0° and 10°, between 10° and 20°, and between 20° and 30°, respectively. The other input parameters of this canopy are listed in Table II. Then, the reflectance is simulated within the aspect range from 0° to 359° in 1° intervals.

Fig. 9 is the reflectance and its corresponding area ratios of the four scene components simulated by GOST. Both the statistical results (see Fig. 8) and the simulated results (see Fig. 9) show that the topographic factors have obvious impacts on the reflectance of sloping canopies. They also show that the simulated reflectance by GOST compares well with that in the TM5 image with the variations of slope and aspect.

TABLE II
MODEL INPUTS FOR SIMULATING THE TM REFLECTANCE

Domain size	1 ha
θ_s'	46°
ϕ_s	154°
θ_v'	0°
ϕ_v	0°
LAI	4
Tree density	2480 trees/ha
Grouping(m2)	4
Quadrat size	$125m^2$
Ha	9.0 m
Hb	4.8 m
r	1.7 m
α	45°
G(θ)	0.5
W_S	0.08 m
γ_E	1.1
Ω_E	0.82
R_T(red)	0.08
R_{ZT}(red)	0.0002
R_T(nir)	0.48
R_{ZT}(nir)	0.0398
R_G(red)	0.04
R_{ZG}(red)	0.0002
R_G(nir)	0.2
R_{ZG}(nir)	0.0284

The reflectance of shaded foliage and background are assumed as constants because multiple scattering schemes are not yet considered in GOST. Therefore, the simulated reflectance of sloping canopies depends on the area ratios of the four scene components at different slopes and aspects. According to a preamble analysis, the gap fraction is invariant at nadir. As a consequence, the area ratio of shaded foliage moves in the opposite direction to the area ratio of sunlit foliage at different aspects, so does the relationship between the sunlit and shaded backgrounds. Furthermore, the simulated reflectance of sloping canopies depends on the area ratios of the sunlit components because the reflectance of the sunlit components is considerably larger than those of the shaded components in both the red and NIR bands. Therefore, the simulated results by GOST show positive correlations between the reflectance of sloping canopies and the area ratios of the sunlit components (see Fig. 9). The negative correlations between the reflectance of sloping canopies and the area ratios of the shaded components are also shown. Although the absolute values of the observed reflectance in the TM5 image and the simulated reflectance of GOST are different, the patterns of the angular variations of the two results are similar, particularly in the NIR band. In the red band, the observed reflectance at slopes from 0° to 10° has no significant difference from those from 10° to 20° because their specific canopy structures are not considered in this experiment. The preamble analysis indicates that the angular variation pattern of the simulated results is compatible with the observed reflectance in theTM5 image (see Fig. 8).

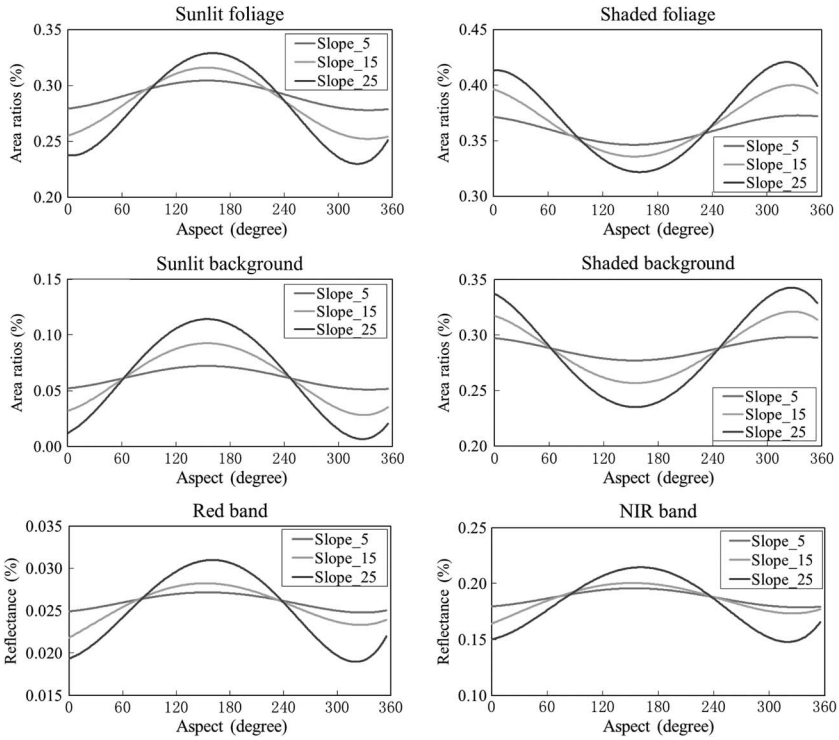

Fig. 9. Simulated four scene components area ratios, red reflectance and NIR reflectance vary with slope and aspect of the terrain by GOST. Slope_5, Slope_15, and Slope_25 are the simulated results of GOST with the slope of the background at 5°, 15°, and 25°, respectively.

Fig. 9 also shows that the area ratios of the sunlit foliage and background reach their maximum values, respectively, and the area ratios of the shaded foliage and background reach their minimum values, respectively, at certain angles on the sunlit slope. (The aspect ϕ_g is about 154°, and the relative azimuth angle between the sun and the sloping background is about 0°.) On the contrary, the area ratios of the shaded foliage and background reach their maximum values and the area ratios of the sunlit foliage and background reach their minimum values at certain angles on the shaded slope. (The aspect ϕ_g is about 334°, and the relative azimuth angle between the sun and the sloping background is about 180°.) Therefore, the maximum and minimum values of reflectance simulated by GOST in both the red and NIR bands appear on the sunlit and shaded slopes for each canopy, respectively. This result is supported by the observed reflectance of the TM5 image.

Furthermore, sunlight can reach more foliage and background on the sunlit slope and less foliage and background on the shaded slope with the increasing slope. Therefore, the canopy reflectance on the sunlit slope increases with slope due to the increasing area ratios of the sunlit foliage and background. On the contrary, the canopy reflectance on the shaded slope decreases with increasing slope due to the increasing area ratios of the shaded foliage and background. It indicates that the variation of the canopy reflectance at a steeper slope is bigger than those at a gentler slope. Both the area ratios of the four scene components and its corresponding reflectance are minimally affected by the topographic factors when the relative azimuth angle between the sunlight and background aspect ϕ_{sg} is about 90°. It is because the topographic factors have the least effects on the area ratios of the four scene components at about 90° ϕ_{sg}. The observed reflectance also supports that bigger and smaller variations of the reflectance are caused by the steeper and gentler slopes, respectively, and the reflectance is minimally affected by the topographic factors at about 90° ϕ_{sg} (see Fig. 8).

The dynamic range of the simulated reflectance is smaller than that in the remote sensing image. This is because 1) the simulation of GOST in this case only considers the topographical variations rather than the variations of canopy parameters, such as LAI and 2) the reflectance of the shaded foliage and background are assumed to be constants in GOST. However, with the support of the observed reflectance in the TM5 image, the simulated results suggest that GOST can capture the major angular variation of the reflectance of sloping canopies.

2) Comparison of the Modeled and MODIS Multiangle Surface Reflectance: In order to further prove the ability of GOST to simulate sloping forest reflectance, an experiment is designed for comparing the simulated multiangle reflectance by GOST with the MODIS surface reflectance. In this experiment, the simulated reflectances with or without considering the topographic factors are compared against MODIS multiangle surface reflectance.

MODIS MOD09GA reflectance data at the 500-m spatial resolution are used for this purpose. A sloping forest location is selected according to slope and aspect maps generated using DEMs downloaded from the U.S. Geological Survey. Cloud-free reflectance values in the red and NIR bands over the course of one month at this location as well as the corresponding solar and view angular data with 1-km spatial resolution are collected for evaluation purposes. The study site is located in Chongqing City, China $(29°37'18.12''\mathrm{N}/107°22'47.28''\mathrm{E})$.

TABLE III
MODEL INPUTS FOR SIMULATING THE MULTIANGLE MODIS SURFACE REFLECTANCE

Domain size	1 ha
Aspect (°)	89°
Slope (°)	20°
θ_s'	27°
ϕ_s	121°
ϕ_v	95°
LAI	4.5
Tree density	1440 trees/ha
Grouping(m2)	4
Quadrat size	125m^2
Ha	6.0 m
Hb	8.5 m
r	1.0 m
α	45°
G(θ)	0.5
Ws	0.09 m
γ_E	1.1
Ω_E	0.8
R_T(red)	0.06
R_{ZT}(red)	0.0001
R_T(nir)	0.5
R_{ZT}(nir)	0.18
R_G(red)	0.15
R_{ZG}(red)	0.0001
RG(nir)	0.25
R_{ZG}(nir)	0.08

Pine (*Pinus massoniana*) is the major conifer species at this study site. Nine cloud-free days from August 1 to 31 of 2011 are selected. The slope is 20° and aspect is 89° from the north.

The input parameters of GOST for this sloping canopy are listed in Table III. In fact, it is difficult to give observation data sets exactly for these 250 000 m^2 (500-m spatial resolution) pixels in the remote sensing images. We have made a best guess to determine the model input using common parameter values of forest within reasonable ranges. The same input parameters are used to simulate the reflectance using GOST with or without considering topographic factors. Therefore, the differences of these modeled results are not derived from these input canopy parameters.

Within these nine cloud-free MODIS observations, there exist one kind of combination of the view azimuth angle, solar azimuth angle, and solar zenith angle. The combination is that the view azimuth angles approximately equaling 95°, the solar azimuth angles approximately equaling 121°, and solar zenith angles approximately equaling 27°. The variation of the view zenith angle is from 1° to 62°. Therefore, with or without considering topographic factors, reflectance values in this plane are simulated according to this angle combination and compared with the MODIS multiangle surface reflectance.

Fig. 10 shows the comparison between the simulated reflectance and MODIS surface reflectance in the red and NIR bands. Generally, the MODIS surface reflectance is closer to the simulated reflectance with considering the topographic factors (slope is 20°) than those without considering the topographic factors (slope is 0°). The dynamic range of the simulated reflectance with considering the topographic factors is close to that of the observed results. However, the dynamic range of the simulated reflectance without considering the topographic factors is underestimated in the red band and overestimated in the NIR band. In the red band, the simulated reflectance without considering the topographic factors is also underestimated. However, it is overestimated in the NIR band at large view zenith angles (view zenith angles larger than 30°). The simulated reflectance with considering the topographic factors appears within reasonable ranges. However, there are still slight differences between the simulated reflectance and MODIS surface reflectance after considering the topographic factors. This can be related to inexact angular matching between the model and the observation, and the approximation of the complex topographical variations within the 500-m pixels with 2-D (smooth and extensive) slopes. This comparison further confirms the ability of GOST in simulating the multiangle reflectance of sloping canopies.

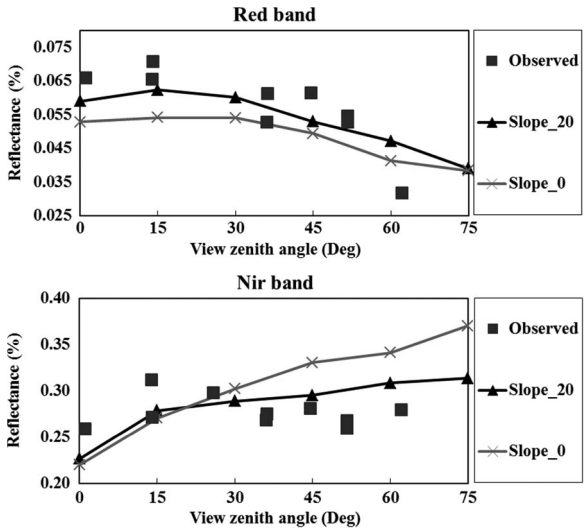

Fig. 10. Simulated multiangle reflectance compared with MODIS surface reflectance at multiple view angles in the red and NIR band. Slope_0 and Slope_20 are the simulated results of GOST with the slope of the background at 0° and 20°, respectively.

IV. CONCLUSION

Based on the four-scale GO model developed for flat terrains, the GOST model in this study is developed to describe the effect of the sloping canopy structure on the reflectance. The following conclusions are drawn from this study.

1) GOST is able to simulate the gap fraction and the ratios of the four scene components (sunlit and shaded canopy fractions and sunlit and shaded background fractions) on sloping terrains. The simulation compares well with the 3-D virtual canopy using a computer graphics technique.
2) GOST provides a useful tool for analyzing remote sensing images over complex terrains. It considerably improves the simulated reflectance in a mountainous area after considering the topographic factors. Model

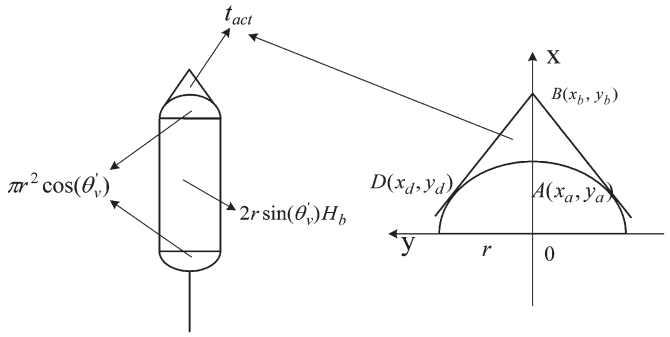

Fig. 11. Projection area t_{act} in the sunlight or viewer directions. t_{act} is in the top part of the "cone + cylinder." $A(x_a, y_a)$, $B(x_b, y_b)$, and $D(x_d, y_d)$ are used for calculating projection area t_{act}.

evaluations against Landsat and MODIS observations demonstrate that the simulated reflectance of GOST over sloping terrains does not have obvious systematic biases. The evaluation against MODIS data also suggests that GOST can simulate multiangle reflectance on sloping forests.

Although it can be improved to include a within-canopy multiple scattering scheme, GOST presented here already has a unique ability to model the bidirectional reflectance distribution of vegetation over sloping terrains. It can also be a useful tool for retrieving canopy parameters using remote sensing images on complex terrains.

APPENDIX
t_{act} GEOMETRY

Projection area t_{act} can be computed by integrating twice from the ellipse to segment $\overline{BD}$ from 0 to y_d (see Fig. 11). Thus

$$\begin{aligned} t_{act} &= 2\int_0^{y_d} \left(\frac{y - b_{BD}}{m_{BD}} - \frac{xa}{r}\sqrt{r^2 - y^2} \right) dy \\ &= 2x_b \cdot y_d - \frac{y_d^2 \cdot \sqrt{x_b^2 - x_a^2}}{r} \\ &\quad - \frac{x_a}{r}\left[y_d \cdot \sqrt{r^2 - y_d^2} + r^2 \cdot \arcsin\left(\frac{y_d}{r}\right) \right] \end{aligned} \quad (23)$$

where b_{BD} is the intercept of segment $\overline{BD}$, and m_{BD} is the slope of segment $\overline{BD}$. x_a, x_b, and y_d can be calculated as follows:

$$\begin{cases} x_a = r \cdot \cos(\theta_v') \\ x_b = r \cdot \sin(\theta_v') / \tan(\alpha) \\ y_d = r \cdot \frac{\sqrt{x_b^2 - x_a^2}}{x_b}. \end{cases} \quad (24)$$

ACKNOWLEDGMENT

The authors would like to thank Dr. Z. Y. Tong and Dr. G. Zheng from Nanjing University, for their help in 3-D virtual modeling. They would also like to thank the two reviewers for their substantial comments.

REFERENCES

[1] X. W. Li and A. H. Strahler, "Geometric-optical modeling of a conifer forest canopy," *IEEE Trans. Geosci. Remote Sens.*, vol. GRS-23, no. 5, pp. 705–721, Sep. 1985.

[2] T. Nilson and U. Peterson, "A forest canopy reflectance model and a test case," *Remote Sens. Environ.*, vol. 37, no. 2, pp. 131–142, Aug. 1991.

[3] C. E. Woodcock, J. B. Collins, V. D. Jakabhazy, X. W. Li, S. A. Macomber, and Y. C. Wu, "Inversion of the Li–Strahler canopy reflectance model for mapping forest structure," *IEEE Trans. Geosci. Remote Sens.*, vol. 35, no. 2, pp. 405–414, Mar. 1997.

[4] F. Deng, J. M. Chen, S. Plummer, M. Z. Chen, and J. Pisek, "Algorithm for global leaf area index retrieval using satellite imagery," *IEEE Trans. Geosci. Remote Sens.*, vol. 44, no. 8, pp. 2219–2229, Aug. 2006.

[5] X. W. Li, A. H. Strahler, and C. E. Woodcock, "A hybrid geometric optical radiative transfer approach for modeling albedo and directional reflectance of discontinuous canopies," *IEEE Trans. Geosci. Remote Sens.*, vol. 33, no. 2, pp. 466–480, Mar. 1995.

[6] W. Ni, X. W. Li, C. E. Woodcock, J. L. Roujean, and R. Davis, "Transmission of solar radiation in boreal conifer forests: Measurements and models," *J. Geophys. Res.*, vol. 102, no. D24, pp. 29 555–29 566, Dec. 1997.

[7] J. M. Chen and S. G. Leblanc, "Multiple-scattering scheme useful for geometric optical modeling," *IEEE Trans. Geosci. Remote Sens.*, vol. 39, no. 5, pp. 1061–1071, May 2001.

[8] J. M. Chen, C. H. Menges, and S. G. Leblanc, "Global mapping of foliage clumping index using multi-angular satellite data," *Remote Sens. Environ.*, vol. 97, no. 4, pp. 447–457, Sep. 2005.

[9] M. Mõttus, M. Sulev, and M. Lang, "Estimation of crown volume for a geometric radiation model from detailed measurements of tree structure," *Ecol. Model.*, vol. 198, no. 3/4, pp. 506–514, Oct. 2006.

[10] D. R. Peddle, R. L. Johnson, J. Cihlar, S. G. Leblanc, J. M. Chen, and F. G. Hall, "Physically based inversion modeling for unsupervised cluster labeling, independent forest classification, and LAI estimation using MFM-5-scale," *Can. J. Remote Sens.*, vol. 33, no. 3, pp. 214–225, Jun. 2007.

[11] M. J. Chopping, L. H. Su, A. Rango, J. V. Martonchik, D. P. C. Peters, and A. Laliberte, "Remote sensing of woody shrub cover in desert grasslands using MISR with a geometric-optical canopy reflectance model," *Remote Sens. Environ.*, vol. 112, no. 1, pp. 19–34, Jan. 2008.

[12] Y. Zeng, M. E. Schaepman, B. F. Wu, J. G. P. W. Clevers, and A. K. Bregt, "Scaling-based forest structural change detection using an inverted geometric-optical model in the Three Gorges region of China," *Remote Sens. Environ.*, vol. 112, no. 12, pp. 4261–4271, Dec. 2008.

[13] Y. Zeng, M. E. Schaepman, B. F. Wu, J. G. P. W. Clevers, and A. K. Bregt, "Quantitative forest canopy structure assessment using an inverted geometric-optical model and up-scaling," *Int. J. Remote Sens.*, vol. 30, no. 6, pp. 1385–1406, Mar. 2009.

[14] M. J. Chopping, L. H. Su, A. Laliberte, A. Rango, D. P. C. Peters, and J. V. Martonchik, "Mapping woody plant cover in desert grasslands using canopy reflectance modeling and MISR data," *Geophys. Res. Lett.*, vol. 33, no. 17, pp. L17402-1–L17402-5, Sep. 2006.

[15] F. Canisius and J. M. Chen, "Retrieving forest background reflectance in a boreal region from Multi-Angle Imaging Spectroradiometer (MISR) data," *Remote Sens. Environ.*, vol. 107, no. 1/2, pp. 312–321, Mar. 2007.

[16] J. Pisek and J. M. Chen, "Mapping forest background reflectivity over North America with Multi-angle Imaging SpectroRadiometer (MISR) data," *Remote Sens. Environ.*, vol. 113, no. 11, pp. 2412–2423, Nov. 2009.

[17] G. Sun and K. J. Ranson, "A three-dimensional radar backscatter model of forest canopies," *IEEE Trans. Geosci. Remote Sens.*, vol. 33, no. 2, pp. 372–382, Mar. 1995.

[18] G. Sun and K. J. Ranson, "Modeling lidar returns from forest canopies," *IEEE Trans. Geosci. Remote Sens.*, vol. 38, no. 6, pp. 2617–2626, Nov. 2000.

[19] W. Ni-Meister, D. L. B. Jupp, and R. Dubayah, "Modeling lidar waveforms in heterogeneous and discrete canopies," *IEEE Trans. Geosci. Remote Sens.*, vol. 39, no. 9, pp. 1943–1958, Sep. 2001.

[20] W. Z. Yang, W. G. Ni-Meister, and S. Lee, "Assessment of the impacts of surface topography, off-nadir pointing and vegetation structure on vegetation lidar waveforms using an extended geometric optical and radiative transfer model," *Remote Sens. Environ.*, vol. 115, no. 11, pp. 2810–2822, Nov. 2011.

[21] D. G. Gu and A. Gillespie, "Topographic normalization of Landsat TM images of forest based on subpixel sun-canopy-sensor geometry," *Remote Sens. Environ.*, vol. 64, no. 2, pp. 166–175, May 1998.

[22] V. R. Kane, A. R. Gillespie, R. McGaughey, J. A. Lutz, K. Ceder, and J. F. Franklin, "Interpretation and topographic compensation of conifer canopy self-shadowing," *Remote Sens. Environ.*, vol. 112, no. 10, pp. 3820–3832, Oct. 2008.
[23] J. Iaquinta and A. Fouilloux, "Influence of the heterogeneity and topography of vegetated land surfaces for remote sensing applications," *Int. J. Remote Sens.*, vol. 19, no. 9, pp. 1711–1723, Jan. 1998.
[24] C. B. Schaaf, X. W. Li, and A. H. Strahler, "Topographic effects on bidirectional and hemispherical reflectances calculated with a geometric-optical canopy model," *IEEE Trans. Geosci. Remote Sens.*, vol. 32, no. 6, pp. 1186–1193, Nov. 1994.
[25] W. Thomas, "A three-dimensional model for calculating reflection functions of inhomogeneous and orographically structured natural landscape," *Remote Sens. Environ.*, vol. 59, no. 1, pp. 44–63, Jan. 1997.
[26] D. L. B. Jupp, J. Walker, and L. K. Penridge, "Interpretation of vegetation structure in Landsat MSS imagery: A case study in disturbed semi-arid eucalypt woodland. Part 2. Model-based analysis," *J. Environ. Manage.*, vol. 23, pp. 35–57, 1986.
[27] J. M. Chen and S. G. Leblanc, "A 4-scale bidirectional reflection model based on canopy architecture," *IEEE Trans. Geosci. Remote Sens.*, vol. 35, no. 5, pp. 1316–1337, Sep. 1997.
[28] F. F. Gerard and P. R. J. North, "Analyzing the effect of structural variability and canopy gaps on forest BRDF using a geometric-optical model," *Remote Sens. Environ.*, vol. 62, no. 1, pp. 46–62, Oct. 1997.
[29] J. R. Dymond and J. D. Shepherd, "Correction of the topographic effect in remote sensing," *IEEE Trans. Geosci. Remote Sens.*, vol. 37, no. 5, pp. 2618–2620, Sep. 1999.
[30] S. A. Soenen, D. R. Peddle, and C. A. Coburn, "SCS+C: A modified sun-canopy-sensor topographic correction in forested terrain," *IEEE Trans. Geosci. Remote Sens.*, vol. 43, no. 9, pp. 2148–2159, Sep. 2005.
[31] B. Combal, H. Isaka, and C. Trotter, "Extending a turbid medium BRDF model to allow sloping terrain with a vertical plant stand," *IEEE Trans. Geosci. Remote Sens.*, vol. 38, no. 2, pp. 798–810, Mar. 2000.
[32] X. W. Li and A. H. Strahler, "Geometric-optical bidirectional reflectance modeling of a conifer forest canopy," *IEEE Trans. Geosci. Remote Sens.*, vol. GRS-24, no. 6, pp. 906–919, Nov. 1986.
[33] J. Franklin and D. L. Turner, "The application of a geometric optical canopy reflectance model to semiarid shrub vegetation," *IEEE Trans. Geosci. Remote Sens.*, vol. 30, no. 2, pp. 293–301, Mar. 1992.
[34] C. E. Woodcock, J. B. Collins, S. Gopal, V. D. Jakabhazy, X. W. Li, S. Macomber, S. Ryherd, V. J. Harward, J. Levitan, and Y. C. Wu, "Mapping forest vegetation using Landsat TM imagery and a canopy reflectance model," *Remote Sens. Environ.*, vol. 50, no. 3, pp. 240–254, Dec. 1994.
[35] X. W. Li and A. H. Strahler, "Modeling the gap probability of a discontinuous vegetation canopy," *IEEE Trans. Geosci. Remote Sens.*, vol. 26, no. 2, pp. 161–170, Mar. 1988.
[36] F. Zhao, X. F. Gu, Q. Liu, T. Yu, L. F. Chen, and H. L. Gao, "Modeling of 3D canopy's radiation transfer in the VNIR and TIR domains," *J. Remote Sens.*, vol. 10, no. 5, pp. 670–675, 2006.
[37] J. L. Song, J. D. Wang, Y. M. Shuai, and Z. Q. Xiao, "The research on bidirectional reflectance computer simulation of forest canopy at pixel scale," *Spectrosc. Spectr. Anal.*, vol. 29, no. 8, pp. 2141–2147, Aug. 2009.
[38] M. I. Disney, P. Lewis, J. Gomez-Dans, D. Roy, M. J. Wooster, and D. Lajas, "3D radiative transfer modelling of fire impacts on a two-layer savanna system," *Remote Sens. Environ.*, vol. 115, no. 8, pp. 1866–1881, Aug. 2011.
[39] J. Neyman, "On a new class of contagious distributions, applicable in entomology and bacteriology," *Ann. Math. Stat.*, vol. 10, no. 1, pp. 35–57, Mar. 1939.
[40] J. Franklin and A. H. Strahler, "Invertible canopy reflectance modeling of vegetation structure in semiarid woodland," *IEEE Trans. Geosci. Remote Sens.*, vol. 26, no. 6, pp. 809–825, Nov. 1988.
[41] M. Rautiainen, P. Stenberg, T. Nilson, and A. Kuusk, "The effect of crown shape on the reflectance of coniferous stands," *Remote Sens. Environ.*, vol. 89, no. 1, pp. 41–52, Jan. 2004.
[42] G. S. Campbell, "Extinction coefficients for radiation in plant canopies calculated using an ellipsoidal inclination angle distribution," *Agr. Forest Meteorol.*, vol. 36, no. 4, pp. 317–321, Apr. 1986.
[43] C. J. Kucharik, J. M. Norman, and S. T. Gower, "Measurements of branch area and adjusting leaf area index indirect measurements," *Agr. Forest Meteorol.*, vol. 91, no. 1/2, pp. 69–88, May 1998.
[44] T. Nilson and A. Kuusk, "Improved algorithm for estimating canopy indices from gap fraction data in forest canopies," *Agr. Forest Meteorol.*, vol. 124, no. 3/4, pp. 157–169, Aug. 2004.
[45] J. M. Chen and T. A. Black, "Defining leaf area index for non-flat leaves," *Plant Cell Environ.*, vol. 15, no. 4, pp. 421–429, May 1992.
[46] J. M. Chen and J. Cihlar, "Plant canopy gap-size analysis theory for improving optical measurements of leaf-area index," *Appl. Opt.*, vol. 34, no. 27, pp. 6211–6222, Sep. 1995.
[47] P. Bourke, 1996. [Online]. Available: http://paulbourke.net/geometry/
[48] A. Simic, J. M. Chen, J. R. Freemantle, J. R. Miller, and J. Pisek, "Improving clumping and LAI algorithms based on multiangle airborne imagery and ground measurements," *IEEE Trans. Geosci. Remote Sens.*, vol. 48, no. 4, pp. 1742–1759, Apr. 2010.

Weiliang Fan received the B.S. degree in horticulture from Shandong Agricultural University, Shandong, China, in 2007 and the M.S. degree in forest management from Zhejiang A&F University, Zhejiang, China, in 2010. He is currently working toward the Ph.D. degree at Nanjing University, Jiangsu, China.

Jing M. Chen received the B.Sc. degree from the Nanjing Institute of Meteorology, Nanjing, China, in 1982 and the Ph.D. degree from Reading University, Reading, U.K., in 1986.

He is a Professor with the Department of Geography and Program in Planning, University of Toronto, Toronto, ON, Canada; a Canada Research Chair; and a Fellow of the Royal Society of Canada. He is also an Adjunct Professor with Nanjing University, Nanjing. He has published over 200 papers in refereed journals, which have been cited over 5000 times in the scientific literature. His major research interests include remote sensing of vegetation and quantifying terrestrial carbon and water fluxes.

Dr. Chen is currently an Associate Editor of the *Journal of Geophysical Research-Atmosphere*, *Canadian Journal of Remote Sensing*, and *Journal of Applied Remote Sensing.*

Weimin Ju received the B.Sc. degree from the Nanjing Institute of Meteorology, Nanjing, China, in 1984 and the M.Sc. and Ph.D. degrees from the University of Toronto, Toronto, ON, Canada, in 2002 and 2006, respectively.

He is currently a Professor with the International Institute for Earth System Sciences, Nanjing University, Nanjing. He has published over 80 papers in refereed journals, including 45 papers in international journals. His major research interests include retrieval of vegetation parameters from remote sensing data and simulating terrestrial carbon and water fluxes.

Gaolong Zhu received the B.S. degree in geography from Beijing Normal University, Beijing, China, in 1997; the M.S. degrees in cartography and geographic information system (GIS) from Peking University, Beijing, in 2003; and the Ph.D. degree in cartography and GIS from Nanjing University, Nanjing, China, in 2011.

He is currently an Associate Professor with the Department of Geography, Minjiang University, Fuzhou, China. His current research interests include modeling and inversion of multiangular remote sensing data.